Solar Energy Materials & Solar Cells 99 (2012) 235–239

Contents lists available at SciVerse ScienceDirect

Solar Energy Materials & Solar Cells

journal homepage: www.elsevier.com/locate/solmat

Ultrathin molybdenum oxide anode buffer layer for organic photovoltaic cells formed using atomic layer deposition

Yu-Chih Tseng, Anil U. Mane, Jeffrey W. Elam*, Seth B. Darling*

Argonne National Laboratory, 9700 S. Cass Ave, Lemont, IL 60439, USA

ARTICLE INFO

Article history:
Received 22 November 2011
Received in revised form
6 December 2011
Accepted 10 December 2011
Available online 26 December 2011

Keywords:
Organic photovoltaics
Hole transport layer
Buffer layer
Atomic layer deposition
Molybdenum oxide

ABSTRACT

In an organic photovoltaic (OPV) cell, the buffer layers connecting the active photovoltaic material to the electrodes strongly influence the overall energy conversion efficiency. In this work, we demonstrate that a thin layer (<4 nm) of MoO_3 formed by atomic layer deposition (ALD) of Mo, followed by oxidation in ozone, performs well as an anode buffer layer in organic photovoltaic cells based on a blend of poly(3-hexylthiophene) and phenyl-C_{61}-butyric acid methyl ester. Compared to the commonly used buffer layer poly(ethylenedioxythiophene):poly(styrenesulfonate) (PEDOT:PSS), the MoO_3 layer causes virtually no degradation in the transmission spectrum. The improvement in optical transmission leads to higher short-circuit current density, and practically the same power conversion efficiency as OPV cells employing PEDOT:PSS. Results from a substantial number of devices indicate that the improvement is statistically significant, demonstrating the reproducibility and reliability of the layer. Moreover, because of the conformal nature of ALD, this approach can be extended to nanostructured systems.

© 2011 Elsevier B.V. All rights reserved.

1. Introduction

Organic photovoltaic (OPV) materials are promising for low-cost [1] solar energy conversion systems deployable over large area [2–6]. A typical (non-inverted) OPV cell design is illustrated in Fig. 1, where the active material is sandwiched between a transparent anode and a metal cathode. A buffer layer is needed between the transparent anode and the active material to facilitate extraction of photogenerated holes, and to ensure that electrons flow into the opposite cathode. This buffer layer enhances the conversion efficiency dramatically. The most commonly used buffer layer is based on poly(ethylenedioxythiophene):poly(styrenesulfonate) (PEDOT:PSS), usually available in aqueous suspension and amenable to solution processing. However, this material is acidic (pH$\sim$1) and can corrode both the substrate material and the processing equipment [7]. In addition, PEDOT:PSS is hygroscopic, and its conductivity can change in the presence of moisture [8]. Its work function is also sensitive to oxygen exposure [9]. Furthermore, PEDOT:PSS degrades significantly at temperatures greater than 250 °C [10], and PEDOT manufacturer additives have both unknown and often deleterious effects [11]. Inorganic anode buffer materials based on metal oxides are generally more stable in an ambient environment and offer an alternative to PEDOT:PSS. Well-known buffer layers include nickel oxide, NiO [12], and vanadium oxide, V_2O_5 [13]. However, these materials need to be deposited under high vacuum and therefore cannot be easily scaled up for large-area manufacturing.

MoO_3 is known to enhance the injection of holes in organic light-emitting diodes (OLEDs) [14,15], and more recently, as an anode buffer layer in OPV cells [16–19]. OPV cells with thermally evaporated MoO_3 have improved reliability in an ambient environment [17], but thermal evaporation is limited to processing in small batches and not scalable for large-area manufacturing. Solution-processed MoO_3 is a possible route to scalable and inexpensive manufacturing [16], but this method suffers from uneven coverage, and the OPV cells do not always have consistent performance. Moreover, no current MoO_3 deposition techniques are compatible with nanostructured substrates [20], which are often applied in PV devices, because they tend to planarize surfaces.

Atomic layer deposition (ALD) is routinely used for many technological applications in part due to its ability to conformally coat surfaces of any geometry, with highly controllable thickness and uniformity over large area. Recent developments in ALD process technology, such as operation at atmospheric pressure [21], also show that this method is potentially useful for large-area processing. In this work, we show that thin films of MoO_3, formed by Mo ALD followed by oxidation in ozone generated under ultraviolet illumination (UV ozone), are highly transparent

* Corresponding authors.
E-mail addresses: jelam@anl.gov (J.W. Elam), darling@anl.gov (S.B. Darling).

0927-0248/$ - see front matter © 2011 Elsevier B.V. All rights reserved.
doi:10.1016/j.solmat.2011.12.004

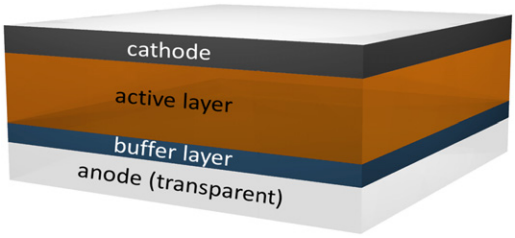

Fig. 1. Schematic of typical OPV device design.

and function well as anode buffer layers. We show also that OPV cells employing ALD MoO_3 thin films have higher short-circuit current density than those using PEDOT:PSS, and that the improvement is statistically significant.

2. Experiment

OPV cells used in this study were prepared on indium tin oxide (ITO) electrodes on glass. As the first step in the fabrication process, the ITO-coated glass slides (Delta Technologies, Ltd.; 10 Ω/sq) were cleaned in an aqueous solution of hydrogen peroxide and ammonium hydroxide at 80 °C for 20 min. Molybdenum was then deposited on the ITO substrates. Uniform and conformal thin films of molybdenum were deposited using Si_2H_6 and MoF_6 precursors at 200 °C by atomic layer deposition (ALD) at a reactor pressure of 1 Torr [22]. The scalability of this Mo ALD process was tested on large substrates (300 mm Si wafers) and the thickness non-uniformity was found to be less than 5%. Following deposition, the Mo film on the ITO substrates was oxidized in UV ozone for 30 min. The substrates were then transferred immediately into a nitrogen glovebox ($O_2 < 0.1$ ppm), where all subsequent fabrication steps were performed.

OPV cells were fabricated by spin-coating the substrates prepared above with Plextronics PV-1000 photoactive ink at 800 rpm for 15 s. The ink was then allowed to dry slowly. The slow-drying process increased the cell efficiency considerably due to higher film crystallinity [23]. The photoactive layer was annealed at 120 °C for 5 min, and a cathode consisting of 30 nm of Ca and 50 nm of Al was deposited using thermal evaporation. The resulting device structure is as illustrated in Fig. 1.

For comparison, OPV cells with PEDOT:PSS as the anode buffer layer were fabricated under the same conditions. ITO slides without Mo were treated in UV ozone for 30 min. A PEDOT:PSS layer (Plextronics PV-1000 hole transport layer) was then spin-coated at 1000 rpm and annealed at 150 °C for 15 min. The active material (Plextronics PV-1000 photoactive ink) was then spin coated at 800 rpm and dried slowly as described above.

For characterization, the OPV cells under test were sealed under a N_2 environment in a small leak-tight chamber with an optical window and electrical feedthroughs to prevent exposure to air during measurement. Device characterization was performed in an Oriel 300 W solar simulator under AM1.5 illumination (1000 W/m^2), supported by a modified Newport IQE-200 quantum efficiency measurement system.

3. Results and discussion

The conformal and uniform coverage of the Mo ALD process is demonstrated in Fig. 2, where the Mo film is shown to cover ALD ITO surfaces conformally over a micromachined trench structure in Si. This is in contrast to previous results using spin-cast MoO_x [16], where the spin-coated film had uneven coverage leading to non-uniform device performance. The ALD Mo film thickness can be precisely controlled as shown in Fig. 3.

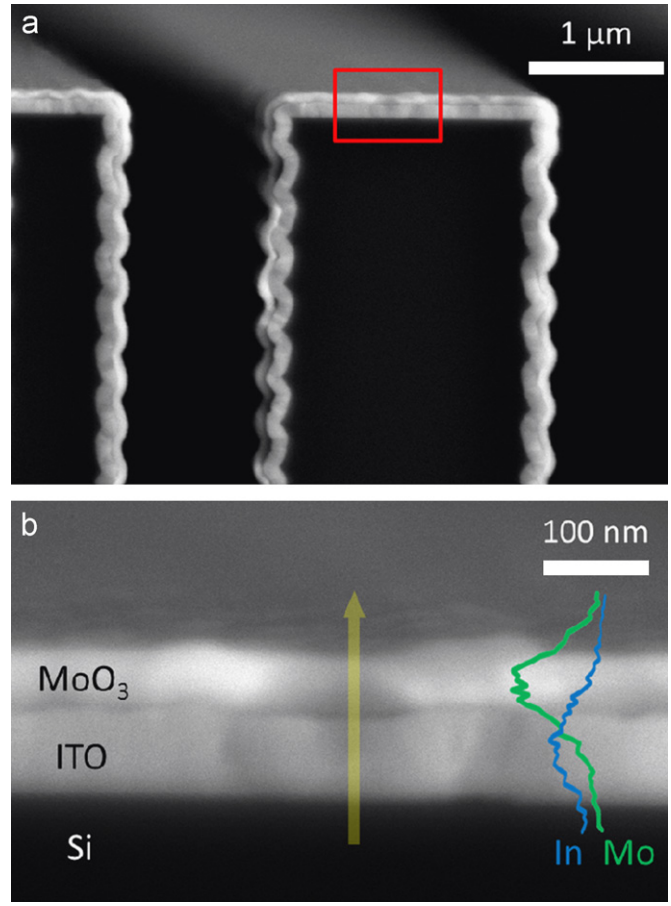

Fig. 2. (a) SEM image of Mo film deposited on ITO-coated micromachined silicon substrate. (b) Energy-dispersive X-ray (EDX) line scan across the films, in region corresponding to the red box in (a). Green: molybdenum signal, Blue: indium signal. The resolution of these EDX data is insufficient to discern whether or not interdiffusion occurs between the buffer layer and the ITO, which would be a potential concern from a long-term device stability standpoint. (For interpretation of the references to color in this figure legend, the reader is referred to the web version of this article.)

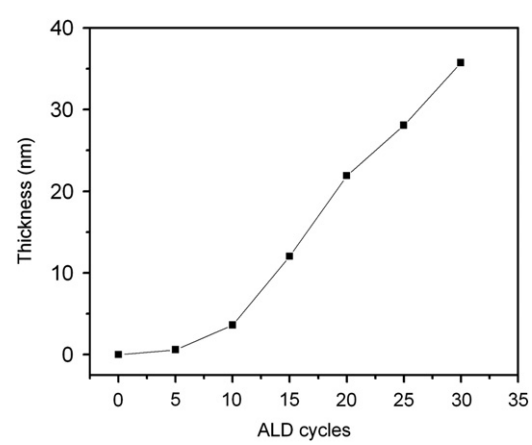

Fig. 3. Thickness of Mo film deposited on ITO as function of ALD cycles determined from four-point probe resistance measurements.

The complete oxidation of the Mo film by UV ozone treatment was confirmed by the XPS spectrum in Fig. S1. A gold film deposited on an adjacent but electrically connected area of the same sample provided the necessary reference (Fig. S1, inset). The

$3d_{5/2}$ peak is shifted from 228 eV to 232 eV, as expected for MoO_3 [24]. The absence of any signal at 228 eV shows that the film is completely oxidized to MoO_3. An optical transmission spectrum of the MoO_3-coated ITO is shown in Fig. 4, and is found to be virtually identical to that of bare ITO. This is in contrast to the PEDOT:PSS-coated ITO, which displays a lower transmission at all wavelengths above 425 nm.

Current–voltage (*J–V*) characteristics of OPV cells prepared with different numbers Mo ALD cycles are shown in Fig. 5. Compared to cells without a buffer layer (Fig. 6, bottom), cells using MoO_3 show a larger open circuit voltage, and significantly higher efficiency. Increasing the number of ALD cycles, corresponding to increased thickness and more complete surface coverage, led to better reproducibility in device performance. Fig. 3 shows that it takes ~5 ALD cycles for Mo to nucleate on the ITO surface before reaching the regime of linear growth. This observation is consistent with the non-uniform coverage and large device-to-device variation encountered in samples with only 2 and 5 cycles of Mo ALD (Fig. 5, top and middle). For devices with sufficient ALD Mo cycles (10 cycles), and hence complete coverage of the ITO substrate, the conversion efficiency is similar to devices processed simultaneously using a PEDOT:PSS buffer layer (Fig. 6, top).

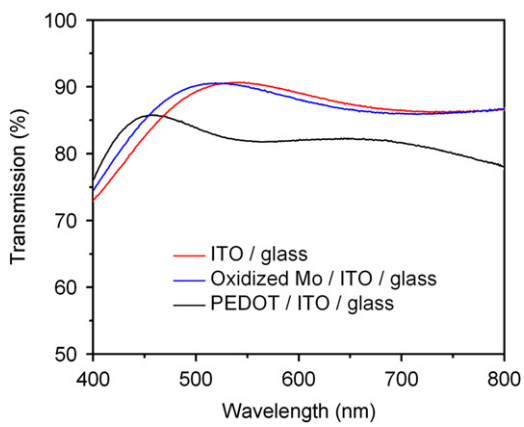

Fig. 4. Transmission spectrum of ITO-coated glass, MoO_3-coated ITO (10 cycles) on glass and PEDOT:PSS (thickness: 70 nm) on ITO-coated glass.

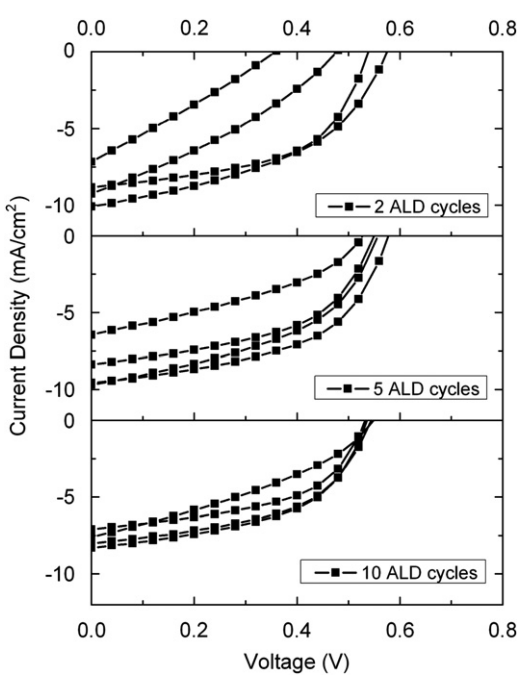

Fig. 5. Current–voltage characteristics of OPV cells made with MoO_3 buffer layer with increasing number of ALD cycles: 2 cycles (top), 5 cycles (middle) and 10 cycles (bottom).

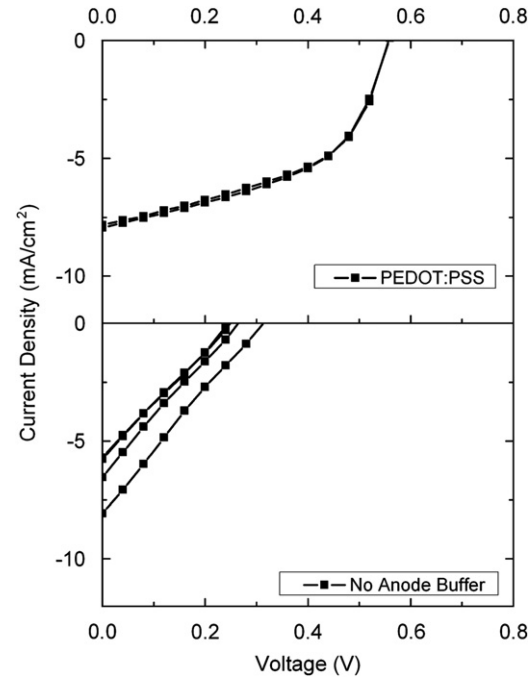

Fig. 6. Current–voltage characteristics of OPV cells made with PEDOT:PSS as the anode buffer layer (top) and no buffer layer between ITO and the active material (bottom).

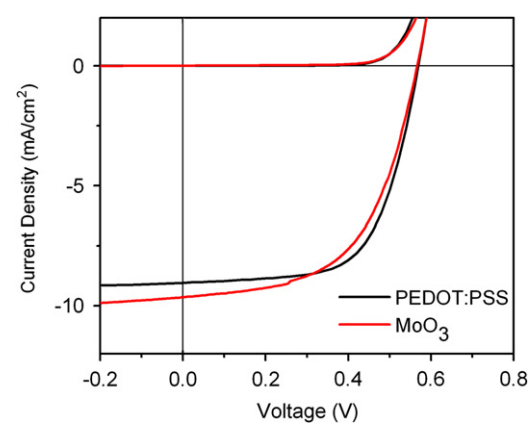

Fig. 7. Average *J–V* characteristics for cells with 10 ALD cycle MoO_3 buffer layer (21 devices) and cells with PEDOT:PSS buffer layer (19 devices).

To rigorously evaluate the difference between PEDOT:PSS and MoO_3 as a buffer layer under optimum processing conditions, a statistically significant number of devices were made and measured. 21 devices with MoO_3 anode buffer layer were compared to 19 devices with PEDOT:PSS. Fig. 7 shows the average *J–V* curves for the two sets of devices. For each set of devices, the average is calculated as the sum of the current from all devices divided by the total area. The device parameters are listed in Table 1. Comparison using analysis of variance (ANOVA) reveals statistically significant differences in the short-circuit current density, the shunt resistance and the series resistance. The improved current density correlates well with the higher optical transmission of the MoO_3 layer (Fig. 4). However, the slightly higher series resistance and lower shunt resistance in cells employing MoO_3

Table 1
Average and standard deviation (in parenthesis) of device parameters of cells employing MoO_3 and those with PEDOT:PSS. Confidence levels are obtained through 2-level analysis of variance (ANOVA). Confidence levels greater than 95% (in bold) indicate statistically significant difference.

	MoO_3	PEDOT:PSS	Confidence level
Power conversion efficiency (%)	3.40 (0.35)	3.28 (0.16)	0.79
Open-circuit voltage (V)	0.567 (0.02)	0.570 (0.004)	0.41
Short-circuit current density (mA/cm^2)	9.6 (0.82)	7.7 (0.38)	~**1**
Fill factor (%)	61.1 (6.4)	63.9 (2.1)	0.92
Specific series resistance (Ω-cm^2)	6.8 (1.4)	4.67 (1.3)	~**1**
Specific shunt resistance (kΩ-cm^2)	851 (450)	1519 (340)	~**1**

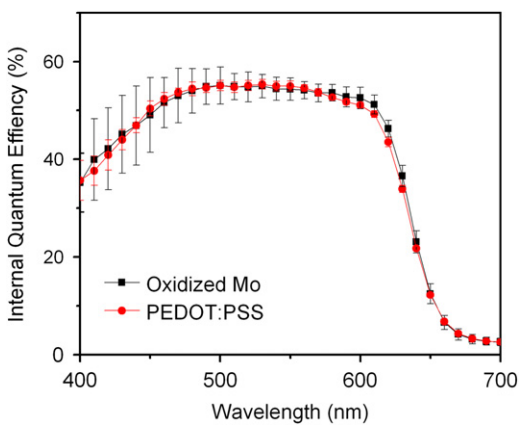

Fig. 8. Internal quantum efficiency measurements for cells with MoO_3 and PEDOT:PSS buffer layer.

led to an overall conversion efficiency that is practically the same as in cells using PEDOT:PSS. It is possible that the energy barrier at the anode/donor electrical contact of MoO_3 is slightly higher, leading to higher R_s. Shunt resistance can result from defect-induced exciton annihilation at the interface, and this may be more prevalent at the interface between MoO_3 compared to PEDOT:PSS. Internal quantum efficiency measurements in Fig. 8 show no appreciable difference between typical devices employing PEDOT:PSS and MoO_3 buffer layers, confirming the essentially similar conversion efficiency between the two sets of devices.

4. Conclusions

Thin films of MoO_3 formed using Mo atomic layer deposition followed by oxidation in UV ozone have been used as anode buffer layers in organic photovoltaic cells, leading to average power conversion efficiency in excess of 3%. There is a statistically significant improvement in short-circuit current density over cells employing the common PEDOT:PSS buffer layer, due to improved optical transmission. The MoO_3 layer has superior optical transmission, conformal coverage, and reproducible performance over a large number of devices. It eliminates the potential for degradation from acidic PEDOT:PSS and, because the film is highly conformal, also enables deposition onto nanostructured substrates. These results show a promising and scalable route for forming a critical layer in low-cost, high-performance OPV cells. ALD, though typically performed in a batch process, has been demonstrated in roll-to-roll processes with flexible substrates and can be performed at atmospheric pressure [25], suggesting its potential integration into OPV manufacturing.

Acknowledgments

The authors thank S. Jokela for expert assistance in acquiring the XPS spectrum, and J. Libera for preparing the ALD ITO films on trenched silicon substrates. Use of the Center for Nanoscale Materials was supported by the U.S. Department of Energy, Office of Science, Office of Basic Energy Sciences, under Contract no. DE-AC02-06CH11357. Elam and Mane were supported by the Argonne-Northwestern Solar Energy Research Center, an Energy Frontier Research Center funded by the U.S. Department of Energy, Office of Science, Office of Basic Energy Sciences under Award number DE-SC0001059.

Appendix A. Supporting information

Supplementary data associated with this article can be found in the online version at doi:10.1016/j.solmat.2011.12.004.

References

[1] S.B. Darling, F. You, T.D. Veselka, A. Velosa, Assumptions and the levelized cost of energy for photovoltaics, Energy and Environmental Science 4 (2011) 3133–3139.
[2] B.C. Thompson, J.M.J. Frechet, Organic photovoltaics—Polymer-fullerene composite solar cells, Angewandte Chemie International Edition 47 (2008) 58–77.
[3] H. Spanggaard, F.C. Krebs, A brief history of the development of organic and polymeric photovoltaics, Solar Energy Materials and Solar Cells 83 (2004) 125–146.
[4] F.C. Krebs, Fabrication and processing of polymer solar cells: a review of printing and coating techniques, Solar Energy Materials and Solar Cells 93 (2009) 394–412.
[5] F.C. Krebs, S.A. Gevorgyan, J. Alstrup, A roll-to-roll process to flexible polymer solar cells: model studies, manufacture and operational stability studies, Journal of Materials Chemistry 19 (2009) 5442–5451.
[6] F.C. Krebs, T. Tromholt, M. Jorgensen, Upscaling of polymer solar cell fabrication using full roll-to-roll processing, Nanoscale 2 (2010) 873–886.
[7] X.H. Yang, F. Jaiser, B. Stiller, D. Neher, F. Galbrecht, U. Scherf, Efficient polymer electrophosphoreseent devices with interfacial layers, Advanced Functional Materials 16 (2006) 2156–2162.
[8] A.M. Nardes, M. Kemerink, M.M. de Kok, E. Vinken, K. Maturova, R.A.J. Janssen, Conductivity, work function, and environmental stability of PEDOT:PSS thin films treated with sorbitol, Organic Electronics 9 (2008) 727–734.
[9] J.S. Huang, P.F. Miller, J.S. Wilson, A.J. de Mello, J.C. de Mello, D.D.C. Bradley, Investigation of the effects of doping and post-deposition treatments on the conductivity, morphology, and work function of poly (3,4-ethylenedioxythiophene)/poly (styrene sulfonate) films, Advanced Functional Materials 15 (2005) 290–296.
[10] B. Friedel, P.E. Keivanidis, T.J.K. Brenner, A. Abrusci, C.R. McNeill, R.H. Friend, N.C. Greenham, Effects of layer thickness and annealing of PEDOT:PSS layers in organic photodetectors, Macromolecules 42 (2009) 6741–6747.
[11] K. Norrman, M.V. Madsen, S.A. Gevorgyan, F.C. Krebs, Degradation patterns in water and oxygen of an inverted polymer solar cell, Journal of the American Chemical Society 132 (2010) 16883–16892.
[12] M.D. Irwin, B. Buchholz, A.W. Hains, R.P.H. Chang, T.J. Marks, p-Type semiconducting nickel oxide as an efficiency-enhancing anode interfacial layer in polymer bulk-heterojunction solar cells, Proceedings of the National Academy of Sciences of the United States of America 105 (2008) 2783–2787.
[13] I. Hancox, L.A. Rochford, D. Clare, P. Sullivan, T.S. Jones, Utilizing n-type vanadium oxide films as hole-extracting layers for small molecule organic photovoltaics, Applied Physics Letters 99 (2011) 013304.
[14] H. You, Y.F. Dai, Z.Q. Zhang, D.G. Ma, Improved performances of organic light-emitting diodes with metal oxide as anode buffer, Journal of Applied Physics 101 (2007) 026105.
[15] W.J. Shin, J.Y. Lee, J.C. Kim, T.H. Yoon, T.S. Kim, O.K. Song, Bulk and interface properties of molybdenum trioxide-doped hole transporting layer in organic light-emitting diodes, Organic Electronics 9 (2008) 333–338.
[16] L. Fengmin, S. Shuyan, G. Xiaoyang, Z. Yun, X. Zhiyuan, Efficient polymer photovoltaic cells using solution-processed MoO_3 as anode buffer layer, Solar Energy Materials and Solar Cells 94 (2010) 842–845.
[17] Y.M. Sun, C.J. Takacs, S.R. Cowan, J.H. Seo, X. Gong, A. Roy, A.J. Heeger, Efficient, air-stable bulk heterojunction polymer solar cells using MoO(x) as the anode interfacial layer, Advanced Materials 23 (2011) 2226–2230.
[18] J.H. Li, J.S. Huang, Y. Yang, Improved hole-injection contact for top-emitting polymeric diodes, Applied Physics Letters 90 (2007) 173505.
[19] P.R. Brown, R.R. Lunt, N. Zhao, T.P. Osedach, D.D. Wanger, L.Y. Chang, M.G. Bawendi, V. Bulovic, Improved current extraction from ZnO/PbS quantum dot heterojunction photovoltaics using a MoO(3) interfacial layer, Nano Letters 11 (2011) 2955–2961.

[20] Y.-C. Tseng, Q. Peng, L.E. Ocola, J.W. Elam, S.B. Darling, Enhanced block copolymer lithography using sequential infiltration synthesis, Journal of Physical Chemistry C 115 (2011) 17725–17729.
[21] J.S. Jur, G.N. Parsons, Atomic layer deposition of Al_2O_3 and ZnO at atmospheric pressure in a flow tube reactor, ACS Applied Materials and Interfaces 3 (2011) 299–308.
[22] D. Seghete, G.B. Rayner, A.S. Cavanagh, V.R. Anderson, S.M. George, Molybdenum Atomic layer deposition using MoF(6) and Si(2)H(6) as the reactants, Chemistry of Materials 23 (2011) 1668–1678.
[23] G. Li, Y. Yao, H. Yang, V. Shrotriya, G. Yang, Y. Yang, "Solvent annealing" effect in polymer solar cells based on poly(3-hexylthiophene) and methanofullerenes, Advanced Functional Materials 17 (2007) 1636–1644.
[24] T.H. Fleisch, G.J. Mains, An XPS study of the UV reduction and photochromism of MoO_3 and WO_3, Journal of Chemical Physics 76 (1982) 780–786.
[25] W.M.M. Kessels, M. Putkonen, Advanced process technologies: Plasma, direct-write, atmospheric pressure, and roll-to-roll ALD, MRS Bulletin 36 (2011) 907–913.